POLISH MARITIME RESEARCH 3(75) 2012 Vol 19; pp. 3-15
10.2478/v10012-012-0026-2

Numerical prediction of steady and unsteady tip vortex cavitation on hydrofoils

Paweł Flaszyński, Ph.D.
Jan A. Szantyr, Prof.
Krzysztof Tesch, Ph.D.
Gdansk University of Technology, Poland

ABSTRACT

The article presents the numerical method for prediction of tip vortex cavitation generated on hydrofoils. This method has been developed in the course of numerical and experimental research described in earlier publications. The objective of the research was to design the optimum discrete grid structure for this specific computational task and to select the best turbulence model for such an application The article includes a short description of the method and a computational example demonstrating its performance. In this example the results of numerical prediction of the cavitating tip vortex obtained from two commercial CFD codes are compared with experimental photographs taken in the cavitation tunnel in the corresponding flow conditions. Altogether nine different flow conditions are tested and analyzed, but only selected results are included. The accuracy of the numerical predictions is discussed and the reasons for minor existing discrepancies are identified. The unsteady tip vortex calculations are also presented, showing the fluctuations of the transverse velocity components predicted for three cross-sections of the cavitating vortex kernel.

Key words: rotary hydraulic machinery; vortex cavitation; numerical methods

INTRODUCTION

The computational method used in this article has been developed in the course of detailed experimental and numerical research described in [2, 3, 4]. This research was at first devoted to numerical prediction of the tip vortices generated behind the tips of hydrofoils without cavitation. At that stage the objective was to reproduce as accurately as possible the complicated velocity field generated by the non-cavitating tip vortices. This velocity field is dominated by the strong secondary flow induced by the vortex and depending on its intensity. The intensity of the tip vortex results from the hydrodynamic loading of the hydrofoil and on the complicated processes of vorticity concentration and dissipation. The results of own LDV measurements of the velocity field in the vicinity of tip vortices behind hydrofoils were used as the reference for the computations. As the result the computational grid structures and turbulence models best suited for prediction of flows dominated by the concentrated vorticity were selected. In the next stage the research was focused on prediction of the detailed geometry of the cavitating tip vortices. In this stage two commercial codes were used in parallel, namely Ansys/Fluent and Ansys/CFX. Analogically to the previous stage, different grid structures and different turbulence models were tested. The PIV measurements of the velocity field around the cavitating tip vortex kernel were used as a support of the numerical calculations. The final recommendations included the optimum grid structure for the specific task of predicting tip vortex cavitation and the turbulence model best suited for this task – k-ε RNG. These recommendations constitute in fact the method for numerical prediction of tip vortex cavitation.

This method is now tested in confrontation with the experimental observations of the tip vortex cavitation behind the hydrofoil. The photograph of the hydrofoil model installed in the measuring section of the cavitation tunnel is shown in Fig. 1, together with the corresponding sketch of the computational domain used in numerical calculations.

Altogether nine different flow conditions were tested. They resulted from combination of three mean flow velocity values of 5.9, 5.2 and 4.3 [m/s] and three angles of attack of 4, 8 and 12 degrees. For the lowest angle of attack only at the highest flow velocity some cavitation phenomena were observed, consequently only seven conditions are presented in detail in the following parts of the article.

NUMERICAL MODEL DESCRIPTION – ANSYS/ FLUENT

Calculations by Ansys/Fluent were performed using the unstructured grid constructed of hexahedral elements, generated using Hexpress Numeca. This grid consists of ~4.7 million

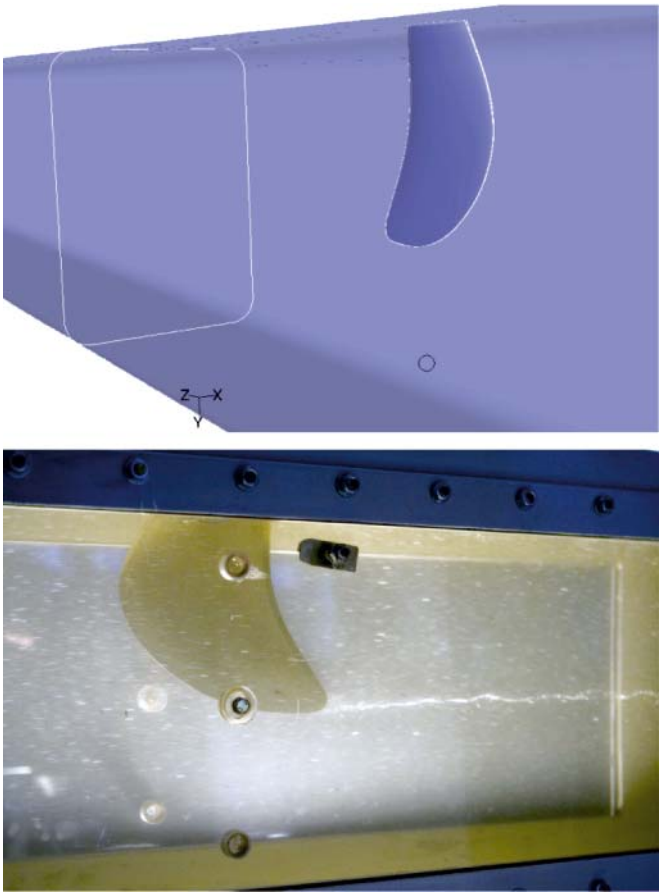

Fig. 1. Scheme of the computational domain and photograph of the hydrofoil in the cavitation tunnel

Fig. 2. Computational grid used in Fluent in the tip region of the hydrofoil

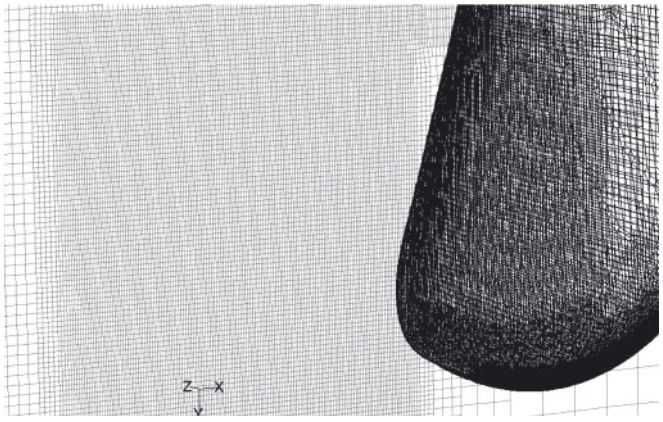

Fig. 3. Computational grid used in Fluent behind the tip region of the hydrofoil

cells and it is refined close to the wall, so the condition $y^+ \sim 1$ is fulfilled. The details of the grid in the most important tip region of the hydrofoil are shown in Figs 2 and 3.

It may be seen that the density of the grid is markedly increased near the leading edge of the hydrofoil and in the region behind the hydrofoil tip, i.e. in the areas playing an important role in the formation of the tip vortex. The computations were performed using the Ansys/Fluent V12 and employing the MUSCL (Monotone Upstream-Centered Scheme for Conservation Laws) scheme for convection terms in the transport equations. The k-ε RNG turbulence model was used, described by the following equations:

$$\frac{\partial}{\partial t}(\rho k)+\frac{\partial}{\partial x_i}(\rho k u_i)= \tag{1}$$
$$=\frac{\partial}{\partial x_j}\left(\alpha_k \mu_{eff}\frac{\partial k}{\partial x_j}\right)+G_k+G_b-\rho\varepsilon-Y_v+S_k$$

$$\frac{\partial}{\partial t}(\rho\varepsilon)+\frac{\partial}{\partial x_i}(\rho\varepsilon u_i)=\frac{\partial}{\partial x_j}\left(\alpha_\varepsilon \mu_{eff}\frac{\partial \varepsilon}{\partial x_j}\right) \tag{2}$$
$$+C_{1\varepsilon}\frac{\varepsilon}{k}(G_k+C_{3\varepsilon}G_b)-C_{2\varepsilon}\rho\frac{\varepsilon^2}{k}-R_\varepsilon+S_\varepsilon$$

Detailed description of the turbulence model and model constants employed in Equations (1) and (2) may be found in [1, 6]. The calculations were performed for a two-phase flow using the mixture model. Cavitation was modeled using the Rayleigh-Plesset equation in Zwart-Gerber-Belamri formulation [7]. The gaseous phase was treated as a compressible medium using the perfect gas equation.

The boundary conditions were set as follows:

Inlet:
- Mass flow according to the mean velocity (4.3, 5.2 or 5.9 [m/s])
- Absolute temperature 283 [K]
- Degree of turbulence 1%
- Ratio of turbulent viscosity to laminar viscosity 10

Outlet:
- Static pressure 15 [kPa] (this corresponds to total pressure in the cavitation tunnel measuring section approximately 30 [kPa])

NUMERICAL MODEL DESCRIPTION – ANSYS/ CFX

Calculations by Ansys/CFX were performed using the unstructured grid which consisted of approximately 9 million elements, including about 8.2 million tetrahedral elements and 0.8 million prismatic elements in the boundary layer. The grid was generated using CFX Mesh. The calculations were performed using Ansys/CFX 12, making use of HRS (High Resolution Scheme) for the convection terms of the transport equations. The details of the grid in the tip region of the hydrofoil are shown in Figs. 4 and 5, with increased density in the regions of expected cavitation.

The calculations by Ansys/CFX were performed for the same flow parameters and boundary conditions as by Ansys/ Fluent. In the case of CFX the gaseous phase was treated as incompressible.

Fig. 4. Computational used in CFX in the tip region of the hydrofoil

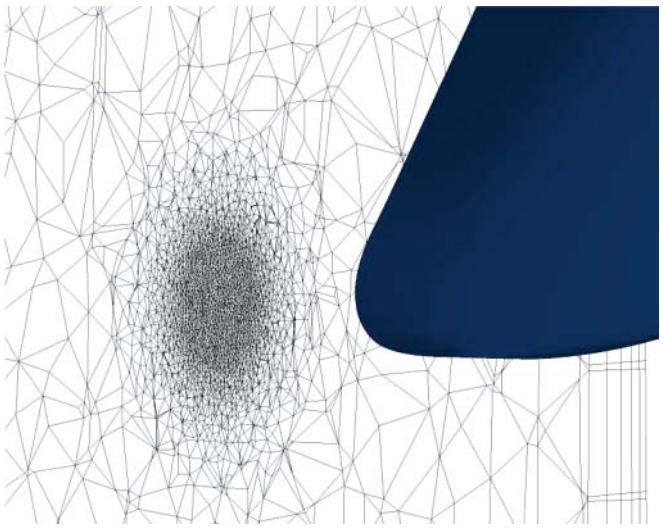

Fig. 5. Computational grid used in CFX behind the tip region of the hydrofoil

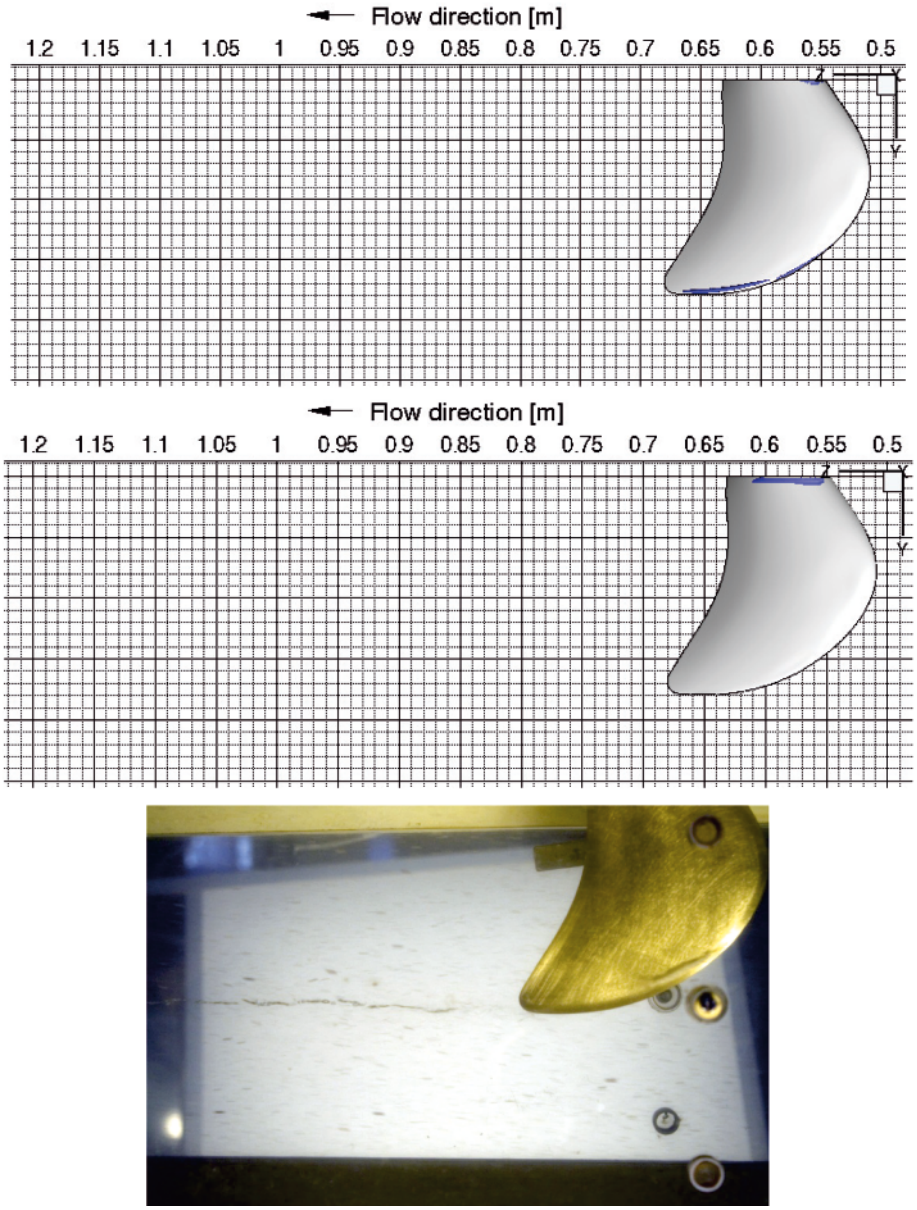

Fig. 6. Comparison of calculations by Fluent (top), CFX (middle) and experimental photograph (bottom) for angle of attack 4 [deg] and mean flow velocity of 5.9 [m/s]

COMPARISON OF NUMERICAL AND EXPERIMENTAL RESULTS

In this section the comparison of numerical and experimental results is shown in Figs. 6 – 12 for seven flow conditions, for which cavitation phenomena were observed. In each Figure the results from Fluent and CFX calculations are shown together with the photograph taken in the cavitation tunnel in the corresponding flow condition.

In Fig. 6 the prediction by Fluent of small region of cavitation area at the tip of the hydrofoil agrees reasonably well with experiment, while both CFX and Fluent do not detect the weak and detached cavitating tip vortex visible in the photograph. Calculation by CFX does not detect any cavitation in tip region of the hydrofoil. A minor root cavitation predicted by both programs is not confirmed by experiment. The reason of such difference is probably a small gap between the hydrofoil and the tunnel upper wall, which influences the flow structure locally. This root gap is not taken into account in the numerical model.

In Fig 7 the calculation by Fluent agrees quite well with the experiment, both the small region of cavitation on the hydrofoil and the presence of the tip vortex are correctly predicted. However, the length of the cavitating tip vortex is seriously underestimated. The calculation by CFX underpredicts both hydrofoil and tip vortex cavitation. The small region of root cavitation indicated by CFX is again not confirmed by experiment.

In Fig. 8, both numerical simulations predict quite long cavitating tip vortices, but they are still shorter than the one observed experimentally. The diameter of the cavitating tip vortex kernel close to the hydrofoil tip is quite well calculated. The prediction of the vortex by CFX is a little further from the experimental one than the prediction by Fluent. On the other hand, the prediction of hydrofoil cavitation by CFX seems to be closer to the observed experimentally, than it is predicted by Fluent. Both programs again calculate small regions of root cavitation, which are not confirmed by experiment.

In Fig. 9 both programs produce practically equivalent predictions, which are quite close to the experimental

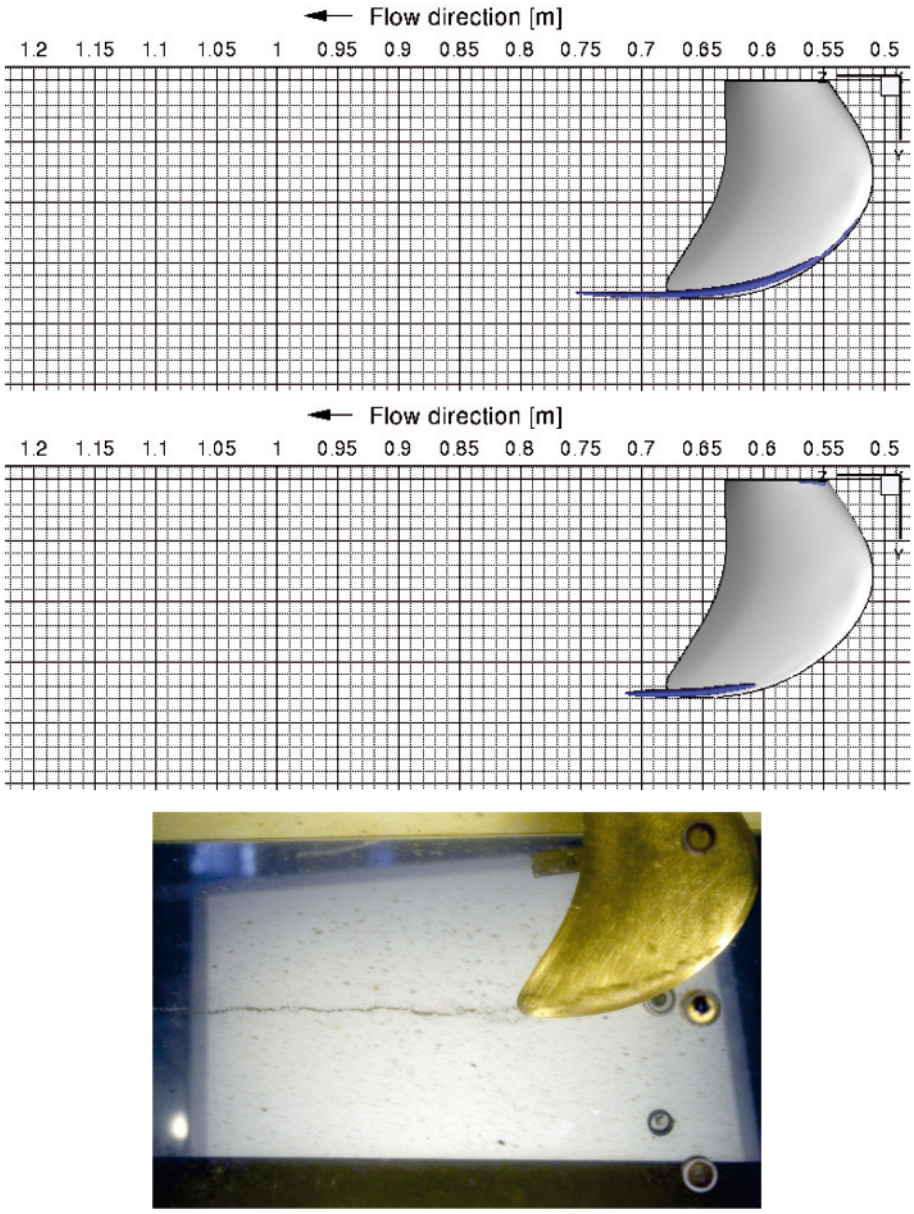

Fig. 7. *Comparison of calculations by Fluent (top), CFX (middle) and experimental photograph (bottom) for angle of attack 8 [deg] and mean flow velocity of 4.3 [m/s]*

observation, both in terms of hydrofoil and tip vortex cavitation. Similarly as before the length of the cavitating tip vortex is underpredicted in calculations. The diameter of the cavitating vortex kernel near the hydrofoil tip is quite well calculated. The abrupt termination of the cavitating vortex kernel as calculated by Fluent looks unnatural. This unnatural vortex termination is due to the ending of the increased density region of the computational grid. In case of Fluent, in order to obtain the converged solution within defined convergence criteria, the tuning of under-relaxation factors was required. The reason for this is the flow separation on the suction side of the hydrofoil and instability caused by the obtained flow structure. The problem is discussed further in the paper.

As previously, the both programs indicate root cavitation, which cannot be seen in the photograph.

At the highest angle of attack (12 deg), differences between CFD results and experimental visualization are the most significant. In Fig. 10, the length of the cavitating tip vortex by both solvers is seriously underpredicted, while its thickness in the region close to the hydrofoil tip is calculated correctly. The abrupt terminations of a thick cavitating vortex in CFX as well as in Fluent look unnatural. This is again caused by the ending of the increased density zone of the computational grid and could be easily corrected if necessary. The radial extent of cavitation on the hydrofoil (along the leading eadge) is reasonable well predicted by both programs. In both cases, the chordwise extent of the cavitation zone is underpredicted.

At the higher velocity (5.2 m/s) and angle of attack equal to 12 deg, the cavitation on the hydrofoil and within the tip vortex is highly overestimated. The radial extent of cavitation on the hydrofoil is well predicted by both programs, but this time they both overestimate the chordwise extent of cavitation. On the other hand, the photographed cavitating tip vortex seems to be visibly thinner than the prediction by both programs. Comparing experimental visualization done for the main flow velocity 4.3 m/s (Fig. 10) and 5.2 m/s (Fig. 11), one can notice that in the second case cavitating vortex seems to be thinner, but less concentrated that at the lower velocity. It arises from the unsteady behaviour of the flow and cavitation conditions

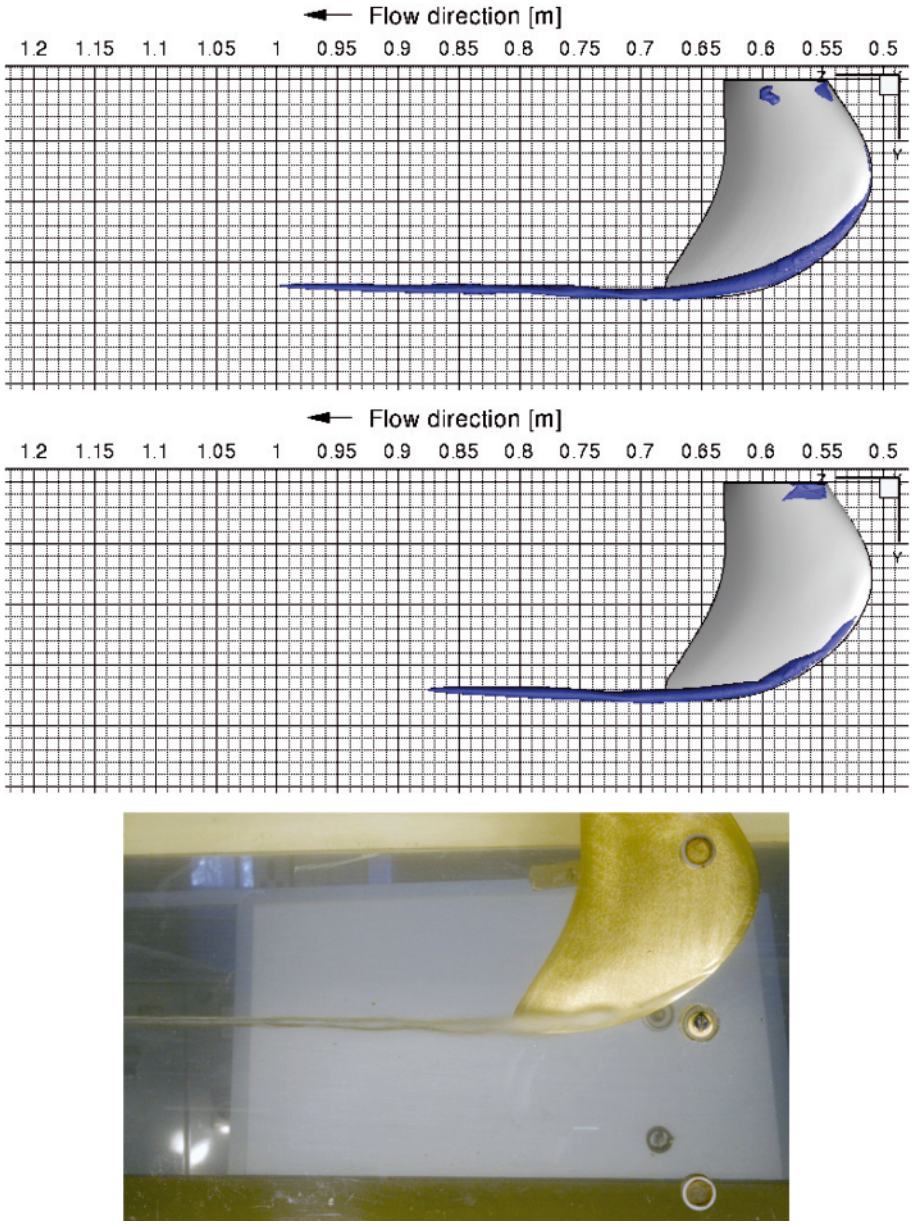

Fig. 8. *Comparison of calculations by Fluent (top), CFX (middle) and experimental photograph (bottom) for angle of attack 8 [deg] and mean flow velocity of 5.2 [m/s]*

high sensitivity and dependence on the local flow structure and water aeration.

The results for the maximum investigated hydrofoil loading (angle of attack 12 [deg], flow velocity 5.9 [m/s]) are not presented, because of lack of Fluent solver convergence caused by the unsteady flow separation on the suction side.

CALCULATIONS OF UNSTEADY TIP VORTEX CAVITATION

It is a well-known fact that cavitation phenomena are inherently unstable. This is particularly true for tip vortex cavitation. Although it was not possible to register the unsteady phenomena in the experiments, an unsteady CFD calculations using Fluent and CFX have been performed in order to compare the steady and unsteady results. The simulations have been performed using the previously selected k - ε RNG turbulence model for the case of inflow velocity 5.2 [m/s] and angle of attack of 12 degrees. In case of both solvers the second order time accurate scheme was applied. The presented below results are obtained for time step 0.01s.

The flow structure based on the time averaged flow field is shown in Fig. 12. The region of calculated flow separation near the root of the hydrofoil and the streamlines starting near the leading edge creating the tip vortex can be observed. Downstream of the hydrofoil, the velocity magnitude at the cross-section is presented. One can notice the increase of the flow velocity close to the tip vortex due to the secondary flow and the decrease of the velocity in the vortex core, as a consequence of the dissipation effects. The lower velocity areas are also shown in the wake and downstream of the suction side separation near the upper wall. The existence of separation is the reason of the convergence problem at the higher hydrofoil loading in Fluent simulations. The effect is weaker in CFX case, because the mesh is much coarser in the area far from the tip vortex, so the vortex structure downstream of the separation dissipates quickly and does not influence on the unsteady behaviour in this flow area.

Anyway, it is interesting that in spite of the lack of the unsteady effect of the separated flow, CFX results indicate higher unsteadiness in the vortex area than it was obtained by

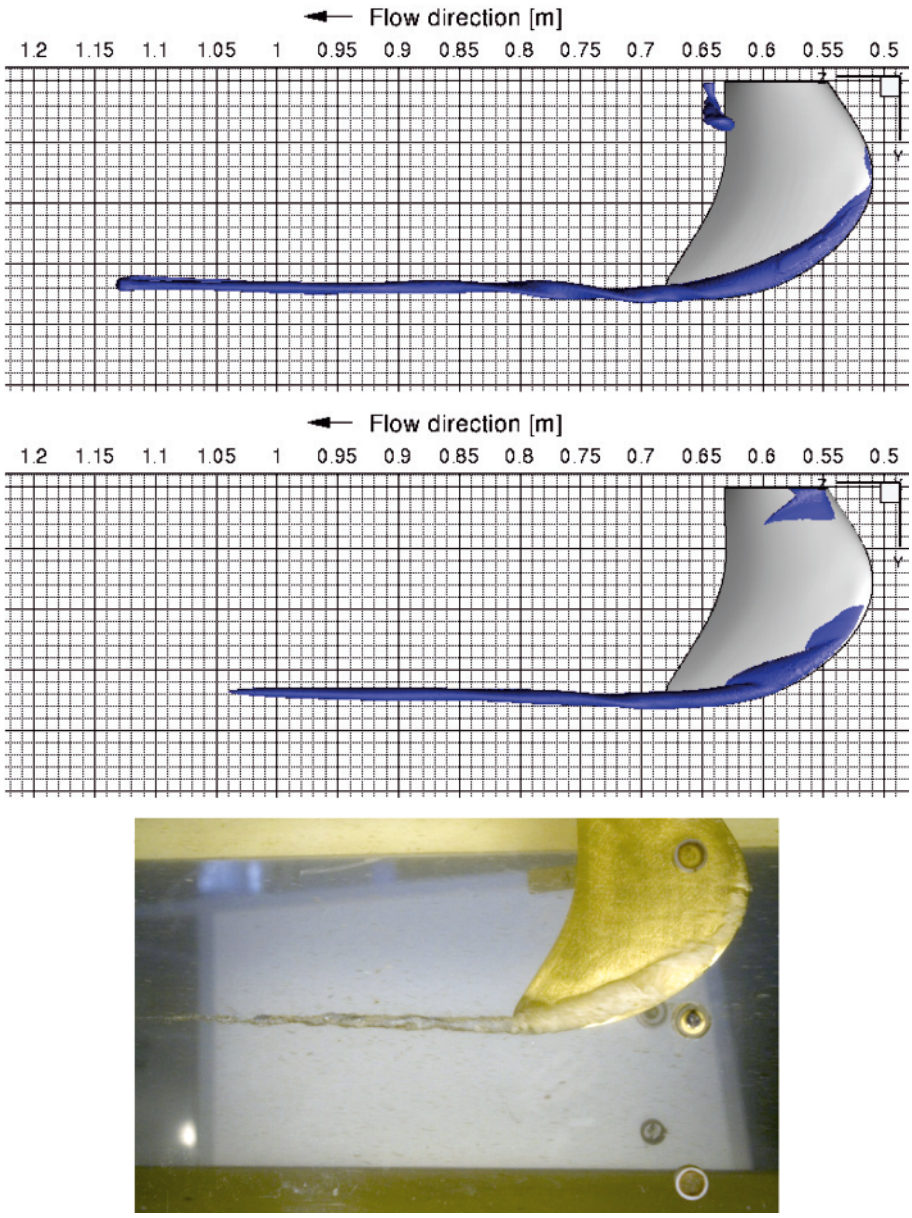

Fig. 9. *Comparison of calculations by Fluent (top), CFX (middle) and experimental photograph (bottom) for angle of attack 8 [deg] and mean flow velocity of 5.9 [m/s]*

Fluent. The fluctuations of the velocity X and Y components at the sections 50 mm, 200 mm and 300 mm downstream of the hydrofoil are shown in Figs. 13 and 14. Both velocity components are located in the secondary flow plane, so they indicate of the fluctuations in the tip vortex area. One can notice, that fluctuations obtained with Fluent simulations are an order of magnitude lower than in CFX case. The simulation time in CFX was 2 seconds and the fluctuations of the tip vortex with 5 Hz frequency are noticed. Fluent simulations were done for much longer time ~20 seconds and no high frequency fluctuations are obtained in the vortex area. The unsteady effects are obtained close to the hydrofoil root only.

In Figs. 13 and 14, the black line marks the area of the time averaged cavitating zone, i.e. the existence of the gaseous phase. In case of Fluent, the flow parameters distribution at the section (50 mm) close to the hydrofoil show the highly three dimensional shape of the cavitating vortex, far from the regular cylindrical shape. Further downstream from the hydrofoil it becomes "more" cylindrical. In case of CFX, such an effect is much weaker.

The next difference is the maximum fluctuations location within the cavitating zone. In the Fluent case, the highest values are spread along the surface dividing the two phases. CFX results indicate the maximum fluctuations at the vortex centre. The experimental assessment of the numerical results accuracy can be done only by the high resolution flow velocity measurements within the range of cavitating vortex. Such measurements were not possible in the research project.

The gaseous phase fluctuations are shown in Fig. 15. As regards the fluctuations distribution, the results are similar. The maximum values are close to the time averaged inter phase border surface in case of both solvers, but CFX values are 7 times higher than obtained in Fluent.

The time averaged secondary flow velocity is shown in Fig. 16. The velocity in plane normal to the main flow indicates the vortex intensity at the consecutive sections downstream of the hydrofoil. It shown that in the gaseous phase zone (or in fact two-phase zone) the velocity is rising from the vortex centre to the location where the gaseous phase disappears, then the velocity decreases in the water

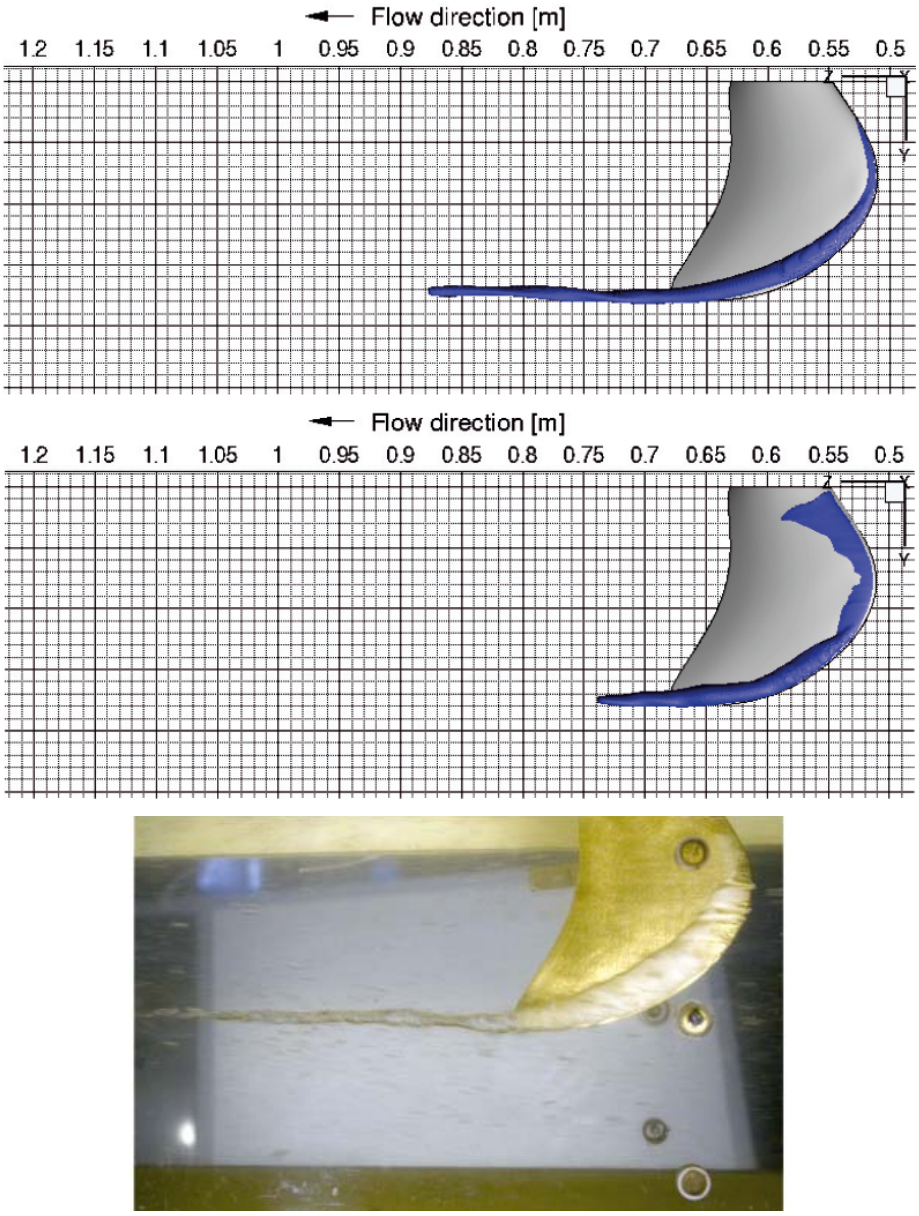

Fig. 10. *Comparison of calculations by Fluent (top), CFX (middle) and experimental photograph (bottom) for angle of attack 12 [deg] and mean flow velocity of 4.3 [m/s]*

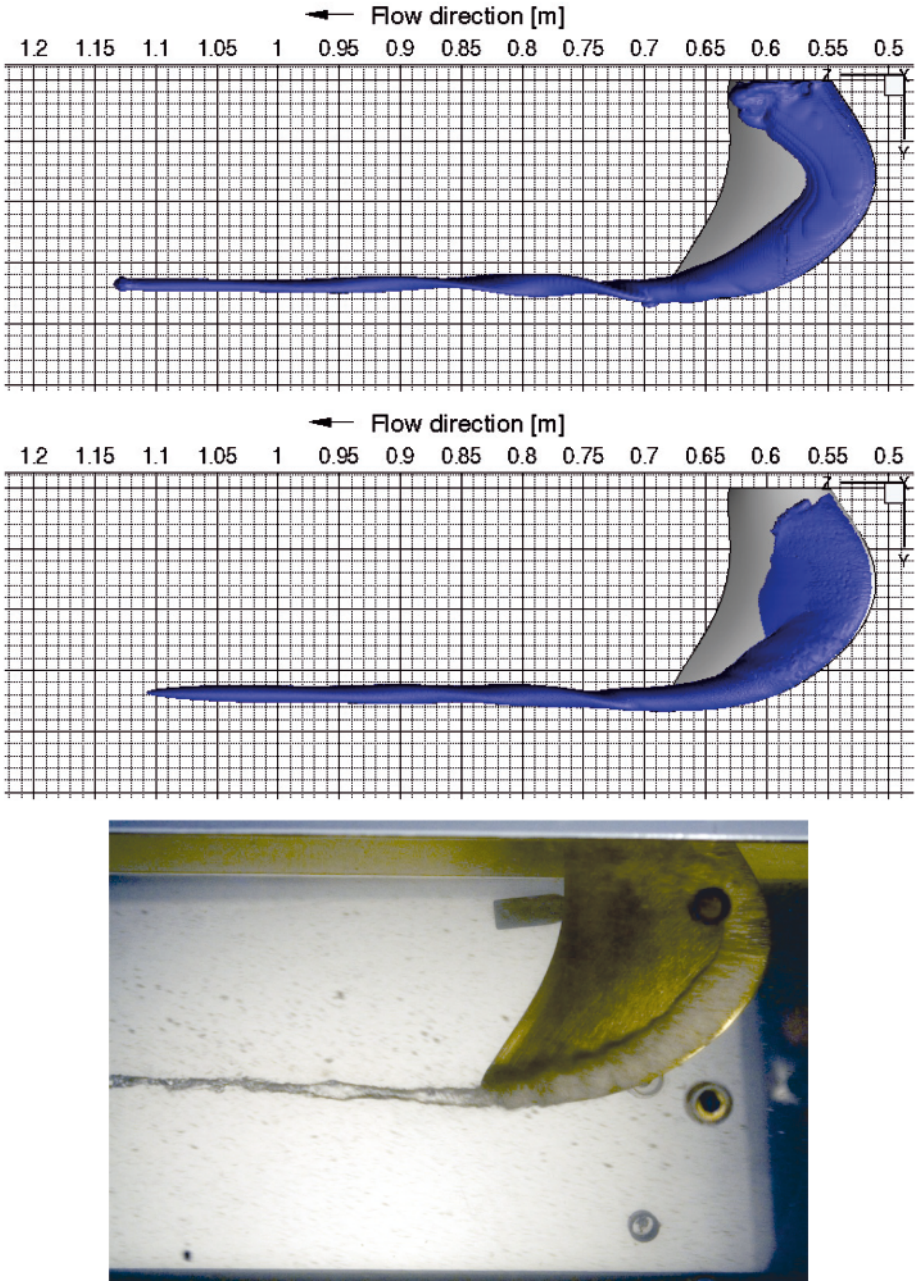

Fig. 11. *Comparison of calculations by Fluent (top), CFX (middle) and experimental photograph (bottom) for angle of attack 12 [deg] and flow velocity of 5.2 [m/s]*

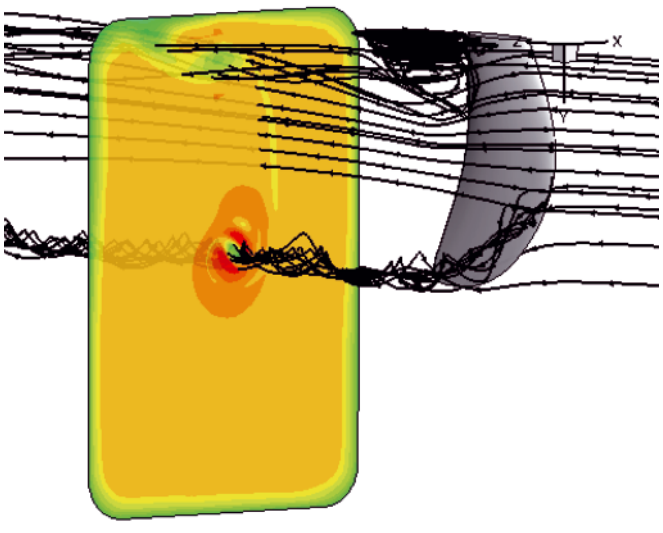

Fig. 12. *Time averaged flow velocity and streamlines (Fluent)*

area. The maximum values obtained in Fluent are higher than in CFX. It means that the vortex intensity predicted by Fluent is higher, what is reflected by the cavitating zone extension. In Fig. 17, the iso-surface of gaseous phase for time averaged results is shown. It can be compared with Fig. 11, where the steady results are presented. In case of CFX, the steady and unsteady results are similar. The unsteady simulations results indicate a bit lower range of cavitation on the hydrofoil and longer cavitating zone in the tip vortex. In case of Fluent results, the difference is much higher. In spite of low fluctuations in the tip vortex area, one can see much smaller extension of the cavitating zone on the hydrofoil. It is now much more closer to the experimental visualization than it was obtained by steady simulations. The higher secondary flow intensity influences the longer tip vortex and the length of cavitation zone. One has to emphasize that three dimensional structure of the vortex and its skewness is also much higher than in steady simulations and both (steady and unsteady) CFX results.

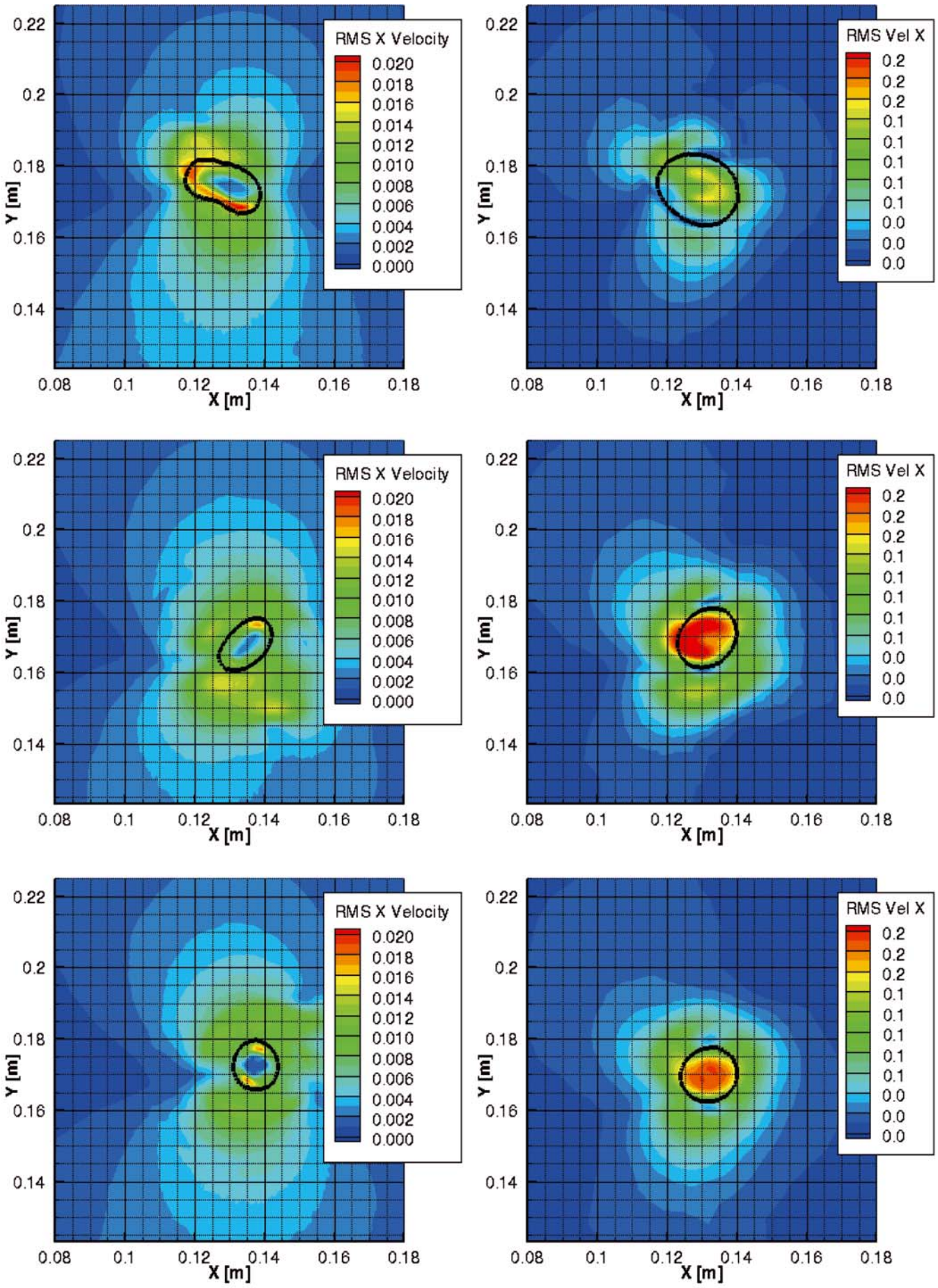

Fig. 13. *The time-dependent fluctuations of the X velocity component (Fluent – left, CFX -right) at the cross-sections (from top) 50 mm, 200 mm and 300 mm behind the hydrofoil (black line indicates the time averaged cavitating zone)*

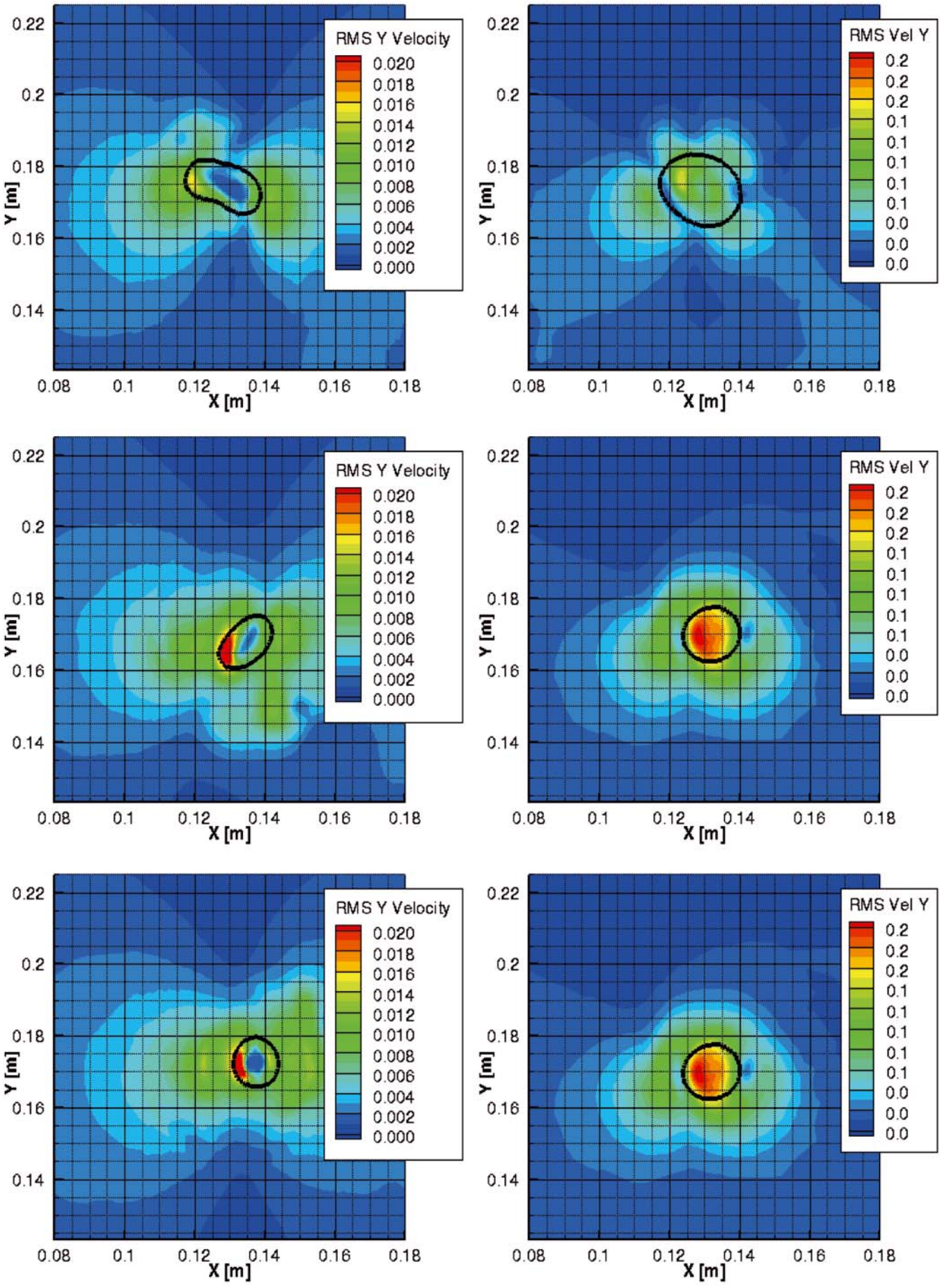

Fig. 14. *The time-dependent fluctuations of the Y velocity component (Fluent – left, CFX -right) at the cross-sections (from top) 50 mm, 200 mm and 300 mm behind the hydrofoil (black line indicates the time averaged cavitating zone)*

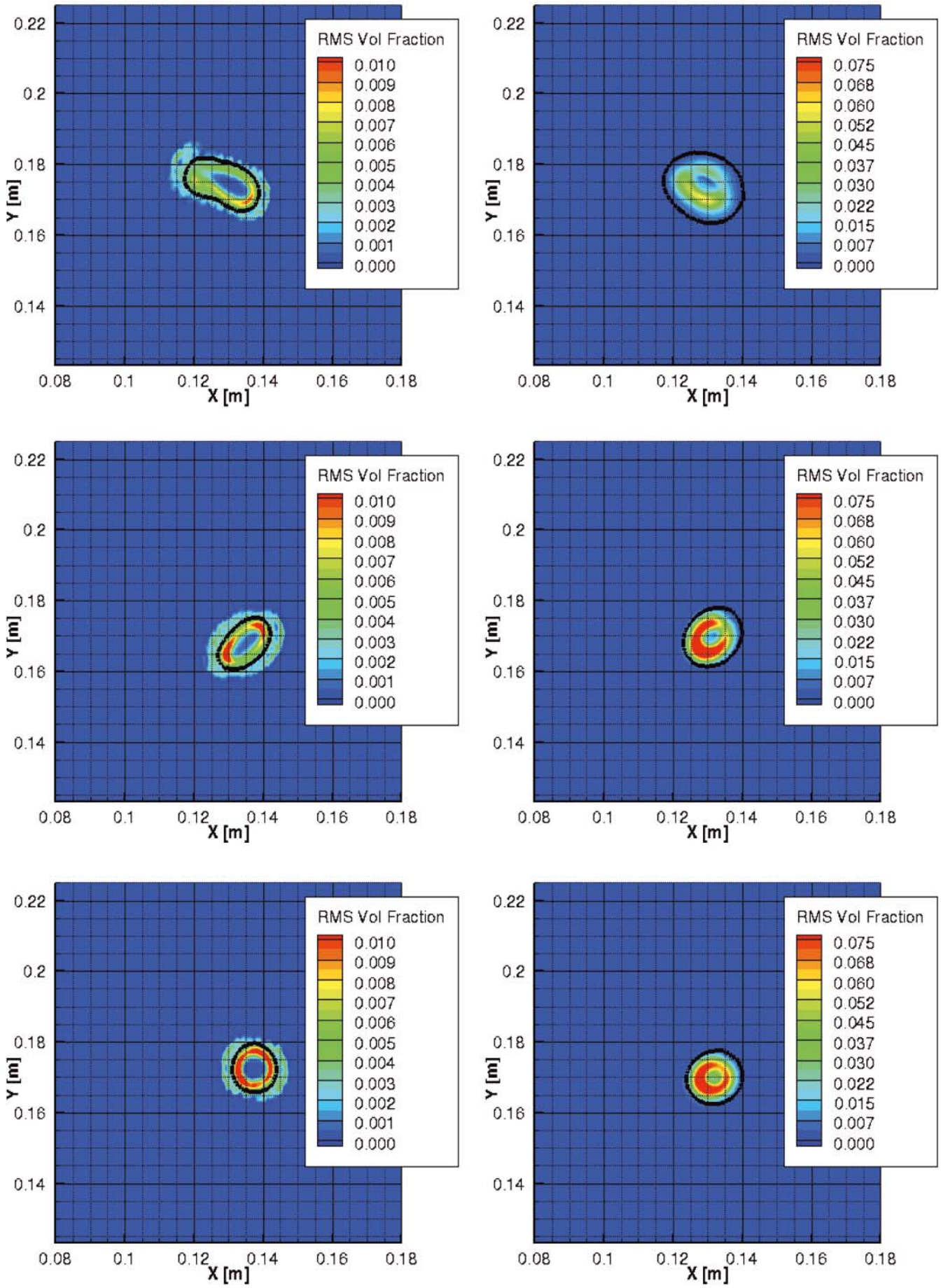

Fig. 15. *The time-dependent fluctuations of the gaseous phase (Fluent – left, CFX -right) at the cross-sections (from top) 50 mm, 200 mm and 300 mm behind the hydrofoil (black line indicates the time averaged cavitating zone)*

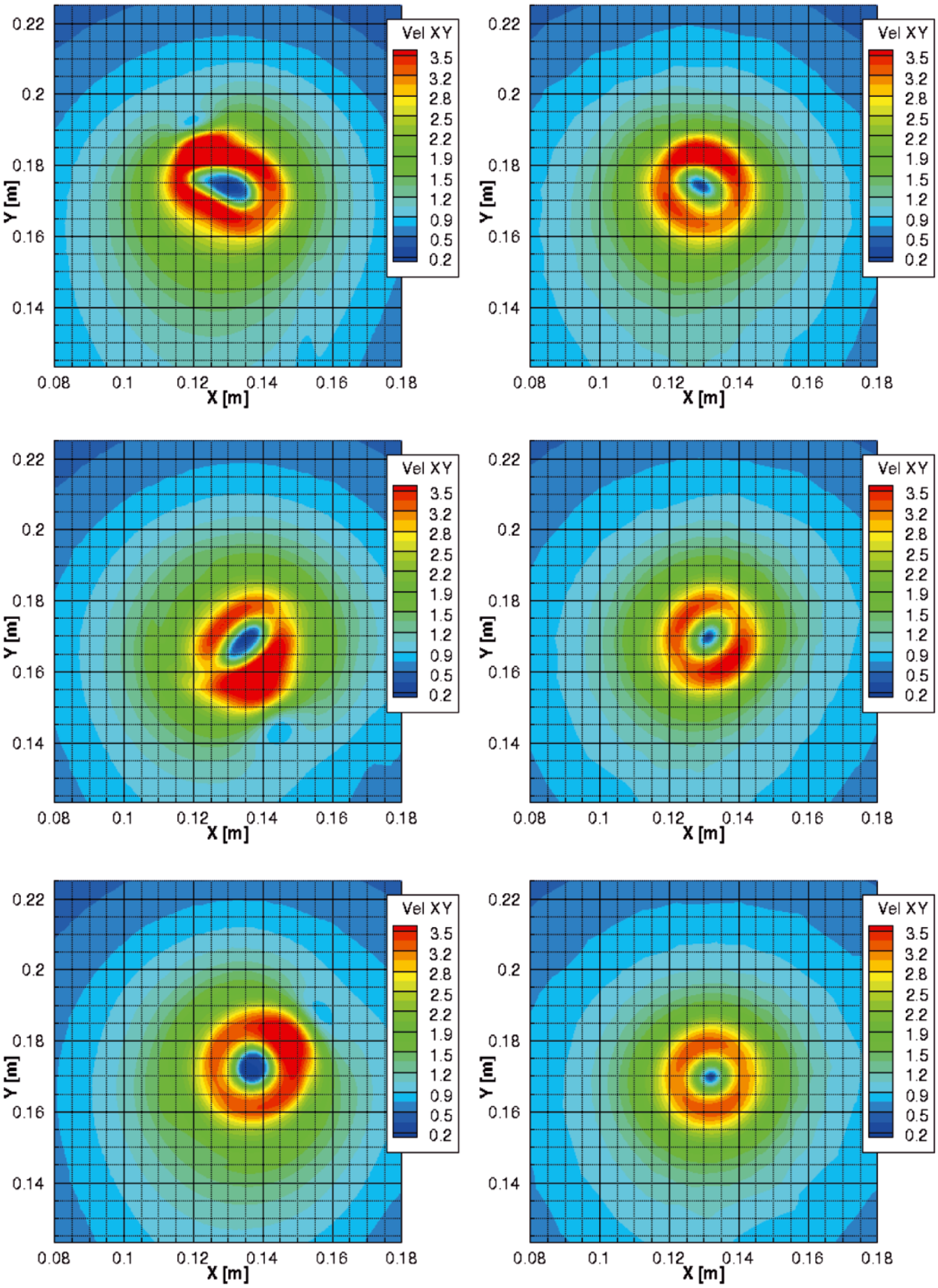

Fig. 16. The time-averaged velocity of flow in the X-Y plane as calculated by Fluent (left) and CFX (right) in the cross-sections (from top) 50 mm, 200 mm and 300 mm behind the hydrofoil

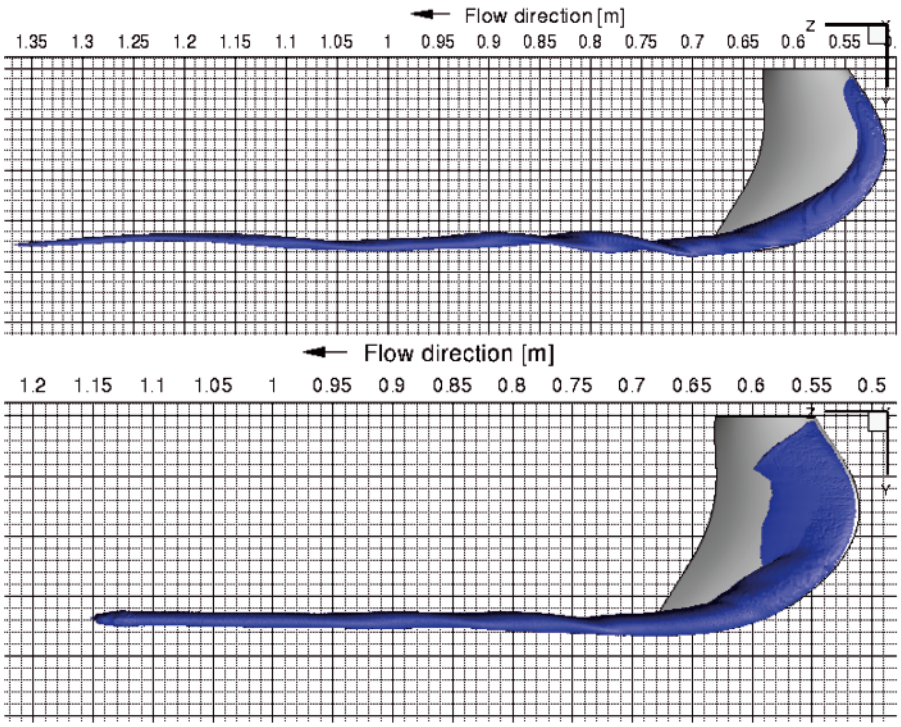

Fig. 17. *Gaseous phase iso-surface (time-averaged) - Fluent (top), CFX (bottom) - angle of attack 12 [deg] and flow velocity of 5.2 [m/s]*

CONCLUSIONS

- The numerical investigations of the cavitating tip vortex generated on the hydrofoil are presented. It is demonstrated that both solvers CFX and Fluent predict the tip vortex and the cavitating zone qualitatively well. In both cases, the trend of dependence of cavitation extent and intensity on the inflow conditions was reflected properly. At high inflow velocity and high angle of attack the separation on the suction side of the hydrofoil was obtained, which is the reason of the instability and the lack of converged solution in Fluent case. The reason of the higher sensitivity to the flow structure dependence in Fluent case is the mesh resolution in the wake along the whole span. In CFX case, the mesh is refined close to the wall and in the tip vortex area, only.
- The simulations for higher loading (high inflow velocity and angle of attack) indicate necessity of the unsteady effects to be taken into account if the highly three dimensional effects are detected in steady simulations. It leads to better agreement with the experimental visualization.
- Since cavitation is highly sensitive and dependent on the local flow structure and water aeration, the quantitative comparison requires detailed information of the fluid quality in order to set an adequate boundary conditions for two phase flow.
- It is difficult to assess the flow velocity distribution in the vortex as well as velocity fluctuations and gas volume fraction, until the high resolution in space and time flow field measurements are not performed.

Acknowledgement

The research described in this article has been conducted with the support of the Research Grant No. N N504 088738 of the Polish National Centre for Research and Development (NCBR).

BIBLIOGRAPHY

1. Ansys/Fluent Release 12.0 Users Manual, 2009
2. Flaszyński P., Szantyr J., Dymarski P., Kraskowski M.: *Numerical Prediction of Vortex Generated by Hydrofoil,* Proc. Intern. Symposium on Marine Propellers, Trondheim, Norway, June 22-24, 2009
3. Flaszyński P., Szantyr J., Biernacki R., Dymarski P., Kraskowski M.: *A Method for the Accurate Numerical Prediction of the Tip Vortices Shed from Hydrofoils*, Polish Maritime Research No. 2(65), Vol. 17, 2010, pp. 10-17
4. Szantyr J.A., Flaszyński P.,Tesch K., Suchecki W., Alabrudziński S.: *An Experimental and Numerical Study of Tip Vortex Cavitation*, Polish Maritime Research No. 4(71), Vol. 18, 2011, pp. 14-22
5. Szantyr J.A., Biernacki R., Flaszyński P., Dymarski P., Kraskowski M.: *An Experimental and Numerical Study of the Vortices Generated by Hydrofoils*, Polish Maritime Research No. 3(61), Vol. 16, 2009, pp. 11-17]
6. Yakhot V., Orszag S.A., Renormalization Group of Turbulence: I. Basic Theory, Journal of Scientific Computing, 1(1):1-51, 1986
7. Zwart P.J., Gerber A.G., Belamri T., *A Two-Phase Flow Model for Predicting Cavitation Dynamics,* Fifth International Conference on Multiphase Flow, Yokohama, Japan, 2004

CONTACT WITH THE AUTHORS

Jan A. Szantyr, Prof., e-mail: jas@pg.gda.pl
Paweł Flaszyński, Ph.D., e-mail: pflaszyn@pg.gda.pl
Krzysztof Tesch, Ph.D., e-mail: krzyte@pg.gda.pl

Faculty of Mechanical Engineering
Gdansk University of Technology
Narutowicza 11/12
80-233 Gdansk, POLAND